



## Short communication

## Highly porous dendritic Ni–Sn anodes for lithium-ion batteries

Kai Zhuo, Myung-Gi Jeong, Chan-Hwa Chung\*

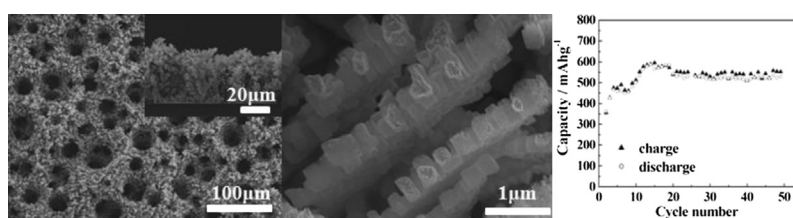
School of Chemical Engineering, Sungkyunkwan University, Suwon 440-746, Republic of Korea



## HIGHLIGHTS

- A porous Ni–Sn foam was fabricated by the electro-deposition accompanied by hydrogen evolution reaction.
- The Ni of the porous and/or dendritic structured Ni–Sn alloy contributed to excellent stability.
- The porous Ni<sub>50</sub>Sn<sub>50</sub> foam exhibited 530 mAh g<sup>-1</sup> capacity after 50 cycles with capacity retention of 90.5%.

## GRAPHICAL ABSTRACT



## ARTICLE INFO

## Article history:

Received 7 November 2012

Received in revised form

4 January 2013

Accepted 5 January 2013

Available online 23 January 2013

## Keywords:

Porous nickel–tin foam

Anode electrode

Hydrogen evolution reaction

Dendrite structures

Lithium-ion battery

## ABSTRACT

A highly porous three-dimensional Ni–Sn alloy foam is fabricated by electro-deposition accompanied by hydrogen evolution reaction. This foam can evolve into porous and dendritic metal alloy structures. These Sn-based electrodes have been evaluated for use as anodes in lithium-ion batteries. Dendritic Ni<sub>50</sub>Sn<sub>50</sub> alloy foam exhibits high electrochemical capacity and excellent cycle stability during charge–discharge processes. The nickel in a Ni–Sn alloy does not break off during the volume expansion/contraction sequence in battery operation cycles and supports the Sn remaining on the anodes. The voids in the tube-like porous Ni–Sn morphology enhance the mass transfer of Li<sup>+</sup> ions and act as mechanical bumpers during the charge–discharge processes.

© 2013 Elsevier B.V. All rights reserved.

## 1. Introduction

Lithium-ion batteries have been widely used as power sources in several digital products, such as cellular phones and portable computers. Most commercial lithium-ion batteries use carbon-based materials for the anodes due to their high safety, good electrical conductivity, high capacity, and low electrochemical potentials as compared with lithium metal [1]. Nowadays, lithium-ion batteries are also considered for use in Electric Vehicles (EVs), Hybrid EVs, and Plug-in Hybrid EVs. For these applications, the safety and powder density of lithium-ion batteries should be improved.

To obtain higher gravimetric and volumetric capacity from Li-ion batteries, tin(Sn)-based intermetallic materials have attracted much interest as replacements for the conventional carbonaceous anode materials of Li-ion batteries, because the Sn in these materials has higher theoretical capacitance (Li<sub>4.4</sub>Sn: 994 mAh g<sup>-1</sup>) than that of graphite (LiC<sub>6</sub>: 372 mAh g<sup>-1</sup>). Pure Sn metal, however, exhibits poor cyclic lifetime due to its mechanical scalability from volume expansion and contraction of the pure Sn metal during lithium insertion and extraction processes. During the charge–discharge cycles, this mechanical scalability will crack and deteriorate the electrode, significantly affecting the mechanical stability and cyclic lifetime of the battery. To solve these problems, two kinds of approaches have been discussed: the use of inactive or active metals as a relatively soft ‘buffer agent’ to relax the volume change of Sn and the size reduction of the particles of tin-based materials to provide space for the volume change of Sn. Many

\* Corresponding author. Tel.: +82 31 290 7260; fax: +82 31 290 7272.

E-mail address: [chchung@skku.edu](mailto:chchung@skku.edu) (C.-H. Chung).

inactive metals have been introduced to enhance the cycle ability of tin-based materials, such as Sn–Fe [2], Sn–Ni [3–7], Sn–Co [3,8–11], and Sn–Cu [12,13].

In our previous works, we have used the electro-deposition accompanied by hydrogen evolution reaction to obtain highly porous metal foams for application to several kinds of electro-catalytic and energy devices. With this fabrication technique, silver, palladium, platinum, and gold porous structures were prepared at high cathodic over-potentials [14–20]. The hydrogen bubbles generated from the conductive substrate at the cathodic over-potential led to the formation of porous and/or dendritic structures. The porous structure is formed by the coalescence of hydrogen bubbles which are detached from the substrate. During this hydrogen evolution reaction as a dynamic template, a metal is co-deposited in the interstitial spaces of the hydrogen bubbles.

In this work, we fabricated porous three-dimensional (3D) Ni–Sn metal foams having particular microforms and dendritic structures with a large surface area by this co-electro-deposition during the hydrogen evolution reaction. The anodic performance of the fabricated Ni–Sn foams in a Li-ion battery has been also evaluated for several different compositions of the Ni–Sn alloy foam electrode.

## 2. Experiment

In preparation of the Ni–Sn metal foam, a Cu foil of 0.5 cm diameter was used as the current collector and conductive substrate for the electro-deposition process. The copper foil was mechanically polished with aluminum powders to describe a smooth surface. The copper oxide on the surface of the Cu foil was then removed by immersing the Cu foil in a 0.1 M sulfuric acid solution for 3 min and then, the Cu foil was cleaned with de-ionized water. A 3D Ni–Sn metal foam was obtained by using an aqueous electrolyte containing 0.2 M  $\text{NiCl}_2$ , 0.015–0.05 M  $\text{SnCl}_2$ , and 1 M  $\text{H}_2\text{SO}_4$  at –4 V cathodic over-potential. All solutions were based on de-ionized water and analytical grade chemicals. The electro-deposition accompanied by hydrogen evolution reaction was carried out at room temperature on a standard three-electrode system consisting of the Cu foil as the working electrode, Pt plate ( $1 \times 4 \text{ cm}^2$ ) as the counter electrode, and Ag/AgCl (3 M NaCl) as the reference electrode using an electrochemical workstation (Electrochemical Impedance Analyzer, IM6ex).

The chemical composition and morphology of the Ni–Sn foam were analyzed by energy dispersive X-ray analysis (EDX) and field emission scanning electron microscopy (SEM) (JEOL, JSM-7000F),

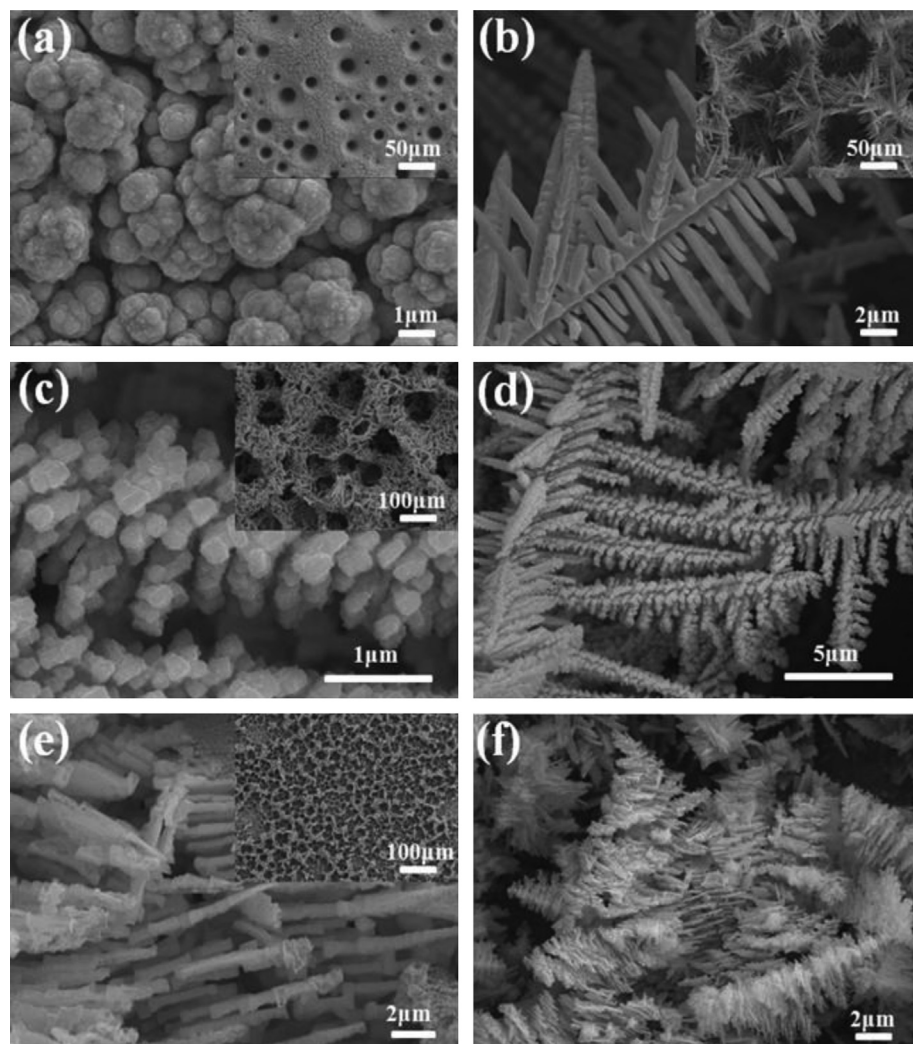


**Fig. 1.** FESEM images of as-deposited porous (a) pure nickel, (b) pure tin, (c), (d)  $\text{Ni}_{20}\text{Sn}_{80}$ , and (e), (f)  $\text{Ni}_{35}\text{Sn}_{65}$ , which were obtained by electro-deposition with hydrogen evolution reaction.

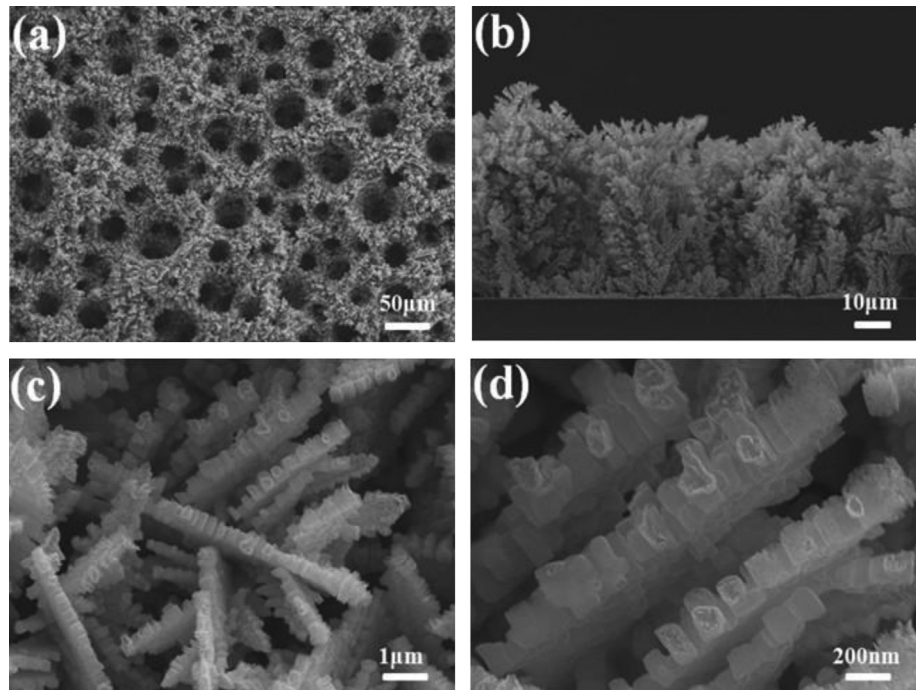


**Fig. 2.** FESEM images of porous Ni<sub>50</sub>Sn<sub>50</sub> alloy foam from (a) top-surface view and (b) cross-sectional view, and (c), (d) their nano-sized tube-like morphologies in Ni–Sn dendrites.

respectively. The structure of the Ni–Sn foam was also examined by using an X-ray diffractometer (XRD) (Bruker AXS with Cu-K $\alpha$  radiation at 40 kV and 40 mA).

### 3. Result and discussion

The Ni–Sn alloy foam to use as the anode electrode in a lithium-ion battery is fabricated by the dynamic hydrogen-template process, in which hydrogen bubbles function as a template in the electro-deposition of metals. These hydrogen bubbles lead to a dendritic morphology by mass transfer in the non-equilibrium condition. Fig. 1 shows FESEM images of pure nickel (*cf.* Fig. 1(a)), pure tin (*cf.* Fig. 1(b)), and 3D porous Ni–Sn alloy foams (*cf.* Fig. 1(c)–(f)). Nickel- and tin-based materials can be formed into self-supporting porous and/or dendritic structures by the dynamic hydrogen-template process, as shown in Fig. 1(a) and (b). Under careful observation, nickel is more likely to become aggregated particles and tin to become needle-type dendrites. The size and numbers of the porous and/or dendritic structures are dependent on the concentrations of the metal ions and hydrogen ions and the applied over-potential.

Fig. 1(c) and (d) shows the FESEM images of Ni<sub>20</sub>Sn<sub>80</sub> alloy foam obtained at −4 V cathodic over-potential with an electrolyte solution containing 0.2 M NiCl<sub>2</sub>, 0.02 M SnCl<sub>2</sub>, and 1 M H<sub>2</sub>SO<sub>4</sub>. The Ni<sub>20</sub>Sn<sub>80</sub> alloy foam has a dendritic morphology similar to that of the pure tin foam. As the tin ion concentration in the solution decreases, the morphology of the Ni<sub>35</sub>Sn<sub>65</sub> alloy foam less similar to the unique needles formation of tin (*refer* Fig. 1(e) and (f)). To obtain a desirable Ni–Sn alloy foam structure which exhibits good electrochemical performances and stability for the Li-ion battery, the composition of Ni<sup>2+</sup> and Sn<sup>2+</sup> needs to be optimized in the electrolyte. In our experiments, a very uniform morphology was obtained when the composition ratio between Ni and Sn was 1:1. Ni<sub>50</sub>Sn<sub>50</sub> alloy foam of this Ni–Sn composition ratio was fabricated at −4 V with an electrolyte containing 0.2 M NiCl<sub>2</sub>, 0.01 M SnCl<sub>2</sub>, and 1 M H<sub>2</sub>SO<sub>4</sub>. As shown in Fig. 2(c) and (d), the Ni<sub>50</sub>Sn<sub>50</sub> alloy

foam has a tube-like dendritic structure, whose tube diameter is less than 100 nm and the length of dendritic branches is about 5  $\mu$ m.

The analysis of the composition ratios of Ni and Sn in Ni–Sn alloy layers of Fig. 2(b) showed a slightly higher atomic percent of nickel at the bottom than at the surface. This phenomenon is caused by the difference in the electrochemical reactivity between nickel and tin due to their different standard electrode potentials. The standard electrode potential of nickel is −0.25 V (vs. SHE), which is a more negative value than the standard electrode potential of tin, which is −0.13 V (vs. SHE). Accordingly, nickel is reduced easily once the electro-deposition begins because it has a lower standard electrode potential than tin.

By X-ray diffraction (XRD), the phases of the nickel, tin, and nickel–tin alloy foams were determined. Fig. 3(a) shows the typical XRD peaks of the porous Ni, Sn, and Ni–Sn(Ni<sub>50</sub>Sn<sub>50</sub>) alloy foams and Fig. 3(b) shows the EDX data of Ni<sub>50</sub>Sn<sub>50</sub>. The pure Sn phases of (200), (101), (220), (211), (112), and (321) are evident at the angles of 30.6, 32.0, 43.9, 44.9, 62.5, and 64.6, whereas the pure Ni phases of (111), (200), and (220) at 44.5, 51.6, and 76.4, respectively. In the alloy, the Ni<sub>3</sub>Sn<sub>4</sub> phases of (111), (310), (202), and (312) are observed at the angles of 30.3, 31.5, 43.8, and 44.2, respectively. (Note that the diffraction peaks at 43.3, 50.4, and 74.1 are the diffraction peaks of the copper foil used as a current collecting substrate.) Shown in Fig. 3, the predominant phase of Ni<sub>3</sub>Sn<sub>4</sub> in the porous Ni–Sn alloy foam slightly deviates from the theoretical XRD data of Ni<sub>3</sub>Sn<sub>4</sub>. The Sn content is higher than 50% by atomic in EDX data. This might be caused by the existence of Ni<sub>x</sub>Sn<sub>y</sub> metastable phases and a small quantity of Ni at the bottom of Ni–Sn alloy foam [6].

Electrochemical charge–discharge behaviors were investigated using home-made Swagelok-fitted cells assembled in an argon-filled glove box. Before measurements, the 3D Ni–Sn alloy foam anodes were dried at 70 °C for 12 h in vacuum. The cathode was utilized with a lithium metal foil, and the electrolyte solution was made of 1 M LiPF<sub>6</sub> in a mixture of ethylene carbonate (EC), dimethyl

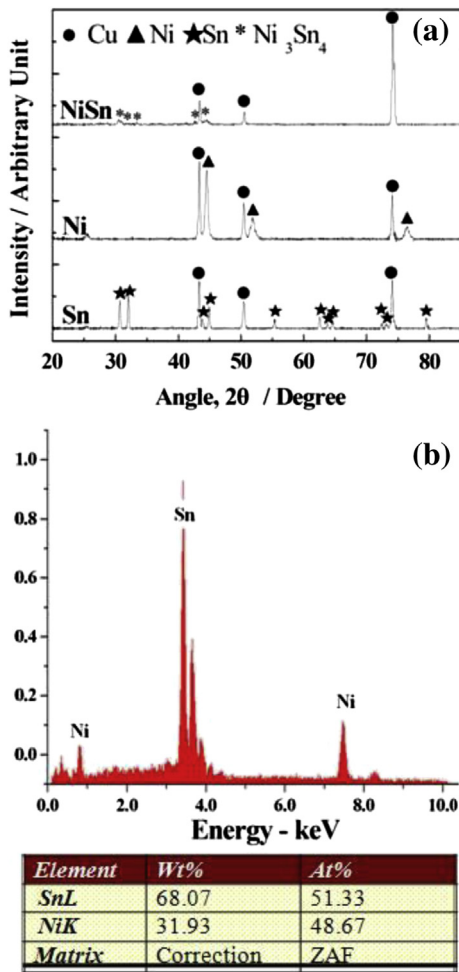
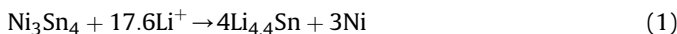


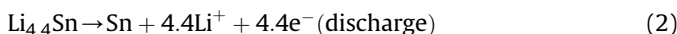
**Fig. 3.** Composition analysis of (a) XRD peaks and (b) typical EDX patterns.

carbonate (DMC), and diethyl carbonate (DEC) with a volumetric ratio of 1:1:1, respectively. The cells were charged and discharged at 1C current density using a battery test system (WPG100 Potentiostat/Galvanostat), and the cut-off voltage range was 0.01–3.0 V (vs. Li/Li<sup>+</sup>) at room temperature. Fig. 4 shows the plots of voltage vs. capacity of the (a) Ni<sub>20</sub>Sn<sub>80</sub> and (b) Ni<sub>50</sub>Sn<sub>50</sub> alloy foams as anodes for a lithium-ion battery at 1C cycling rate. During the first charge, the Li insertion into the Ni–Sn alloy occurred at lower than 0.5 V vs. Li/Li<sup>+</sup>. A clear potential plateau was shown at around 0.5 V vs. Li/Li<sup>+</sup> in the first cycle, which is caused by the lithiation process into Sn to form the Li<sub>x</sub>Sn alloy [3–6,8]. The expression is described by the following reactions [6]:

First cycle:



Following cycles:



The crystal structure of Li<sub>x</sub>Sn changes by the change of *x* value in charge cycles. The Ni<sub>3</sub>Sn<sub>4</sub> phase is formed again during the discharge process [21].

In Fig. 5, the initial discharge capacities of Ni<sub>20</sub>Sn<sub>80</sub> and Ni<sub>50</sub>Sn<sub>50</sub> are 496 mAh g<sup>-1</sup> and 361 mAh g<sup>-1</sup>, respectively. A higher Sn content seems to lead a higher initial discharge capacity. These

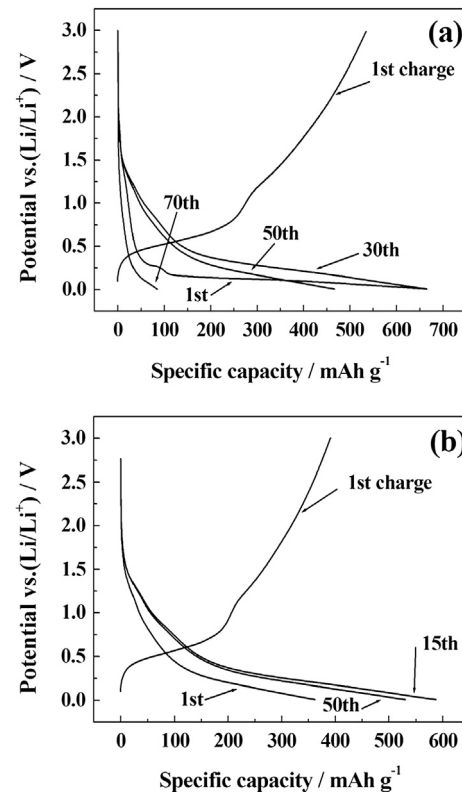


**Fig. 4.** First charge route and the discharge potential profiles of (a) Ni<sub>20</sub>Sn<sub>80</sub> and (b) Ni<sub>50</sub>Sn<sub>50</sub> at 1C rate.

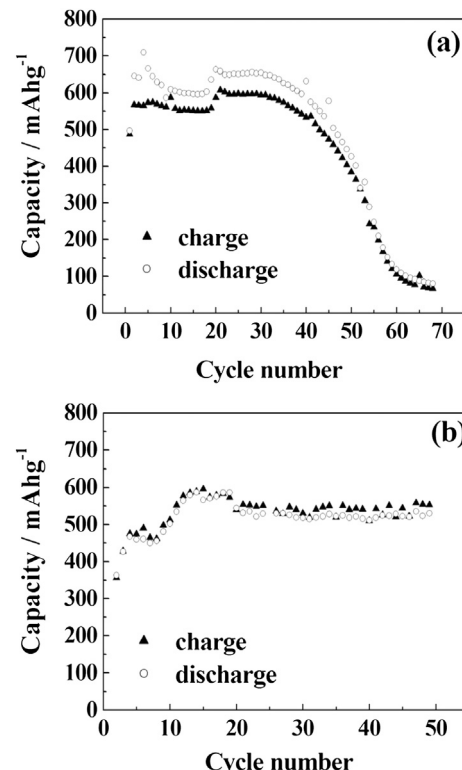


**Fig. 5.** Anodic capacity performances of (a) Ni<sub>20</sub>Sn<sub>80</sub> and (b) Ni<sub>50</sub>Sn<sub>50</sub> at 1C rate.

discharge capacities are generally higher than the charge capacity because the charge process usually undergoes in full charging. In charge–discharge cycling, charge mode is continued to combine Li<sup>+</sup> with Sn for composition of Li<sub>4.4</sub>Sn until constant time after arrival at 3 V. On the other hand, Li<sup>+</sup> inserted into Ni–Sn alloy might not be sufficiently extracted from the Li<sub>4.4</sub>Sn. For these reasons, some cases of discharge capacity showed higher than a corresponding charge capacity. After 50 cycles, however, the capacity of the Ni<sub>50</sub>Sn<sub>50</sub> anode increases to 530 mAh g<sup>-1</sup> and it remains, whereas that of Ni<sub>20</sub>Sn<sub>80</sub> is 426 mAh g<sup>-1</sup> at the 50th cycle but decreases down to 107 mAh g<sup>-1</sup> at the 60th cycle. The capacity of Ni<sub>50</sub>Sn<sub>50</sub> is retained at 90.5% (compare to the maximum capacity of discharge) even after 50 cycles. This value is higher than those for other reports about nano-structure of Sn-based materials [5,22].

It could be concluded that the nickel in the Ni–Sn alloy contributes as a buffer agent that improves the mechanical property of the anode in charge–discharge cycles so that it yields better electrochemical performance in battery applications. During the repeated Li<sup>+</sup> insertion and extraction reaction, nickel plays an important role in keeping the stability of Ni–Sn anode materials, as evident in the rapid decrease of capacity of Ni<sub>20</sub>Sn<sub>80</sub> and the excellent stability of Ni<sub>50</sub>Sn<sub>50</sub> (cf. Fig. 5). A sufficient amount of nickel in an Ni–Sn alloy foam prevents the breaking-off of the tin metal from the electrode substrate due to volume expansion and contraction during charge–discharge cycles.

In addition, due to the highly porous 3D Ni–Sn structure, Li<sup>+</sup> ions can be inserted themselves into the tube-like porous dendritic surface promptly, which lowers the mass-transfer limitation and increases the energy density of the electrodes. The voids in the porous anode layers can not only enhance the accessibility of Li ions but also moderate as a mechanical bumper, in response to volume changes during the charge–discharge processes to prevent cracks and disintegration of the Ni–Sn alloy. Accordingly, the nano-sized tube-like porous Ni–Sn morphology significantly influences the performance of the charge–discharge because of its effect on mass transfer and its role as a mechanical moderator.

#### 4. Conclusions

The 3D porous dendritic Ni–Sn alloy foam was electro-deposited within a dynamic hydrogen-bubble template. Nano-sized tube-like dendritic features were prepared and utilized as anodes in Li-ion batteries. A sufficient amount of nickel in a Ni–Sn anode is needed to maintain capacity value of Li-ion battery even

after repeated charge–discharge cycles. The highly porous structure of the Ni–Sn anode contributes to excellent cycle-life stability, providing facile accessibility to Li<sup>+</sup> ions. These volumetric voids also act as mechanical bumpers preventing the structural disruption of Ni–Sn anodes. The porous Ni<sub>50</sub>Sn<sub>50</sub> alloy foam exhibited 530 mAh g<sup>-1</sup> capacity at 1C current density, and the capacity is retained at 90.5% (compare to the maximum capacity of discharge) even after 50 cycles.

#### Acknowledgments

This research was supported by the Basic Science Research Program through the National Research Foundation of Korea (NRF) funded by the Ministry of Education, Science and Technology (2012-0001525).

#### References

- [1] J.O. Besenhard (Ed.), *Handbook of Battery Material*, Wiley-VCH, New York, 1999.
- [2] J.-M. Lee, W.-S. Chang, B.-C. Yu, H. Kim, D. Im, S.-G. Doo, H.-J. Sohn, *Electrochim. Commun.* 12 (2010) 928–993.
- [3] S.-W. Woo, N. Okada, M. Kotobuki, K. Sasajima, H. Munakata, K. Kajihara, K. Kanamura, *Electrochim. Acta* 55 (2010) 8030–8035.
- [4] Zhang Da-wei, Yang Chen-ge, Dai Jun, Wen Jian-wu, Wang Long, Chen Chun-hua, *Trans. Nonferrous Met. Soc. China* 19 (2009) 1489–1493.
- [5] K. Nishikawa, K. Dokko, K. Kinoshita, S.-W. Woo, K. Kanamurad, *J. Power Sourc.* 189 (2009) 726–729.
- [6] J. Hassoun, S. Panero, B. Scrosati, *J. Power Sourc.* 160 (2006) 1336–1341.
- [7] H.-R. Jung, E.-J. Kim, Y.J. Park, H.-C. Shin, *J. Power Sourc.* 196 (2011) 5122–5127.
- [8] L.-J. Xue, Y.-F. Xu, L. Huang, F.-S. Ke, Y. He, Y.-X. Wang, G.-Z. Wei, J.-T. Li, S.-G. Sun, *Electrochim. Acta* 56 (2011) 5979–5987.
- [9] J.-T. Li, S.-R. Chen, F.-S. Ke, G.-Z. Wei, L. Huang, S.-G. Sun, *J. Electroanal. Chem.* 649 (2010) 171–176.
- [10] X.-Y. Fan, F.-S. Ke, G.-Z. Wei, L. Huang, S.-G. Sun, *J. Alloy. Compd.* 476 (2009) 70–73.
- [11] G. Ferrara, L. Damen, C. Arbizzani, R. Ingua, S. Piazza, C. Sunseri, M. Mastragostino, *J. Power Sourc.* 196 (2011) 1469–1473.
- [12] L. Xue, Z. Fu, Y. Yao, T. Huang, A. Yu, *Electrochim. Acta* 55 (2010) 7310–7314.
- [13] J.Y. Kwon, J.H. Ryu, Y.S. Jung, S.M. Oh, *J. Alloy. Compd.* 509 (2011) 7595–7599.
- [14] S. Cherevko, C.-H. Chung, *Electrochim. Acta* 55 (2010) 6383–6390.
- [15] S. Cherevko, X. Xing, C.-H. Chung, *Electrochim. Commun.* 12 (2010) 467–470.
- [16] S. Cherevko, N. Kulyk, C.-H. Chung, *Nanoscale* 4 (2012) 103–105.
- [17] S. Cherevko, X. Xing, C.-H. Chung, *Appl. Surf. Sci.* 257 (2011) 8054–8061.
- [18] S. Cherevko, N. Kulyk, C.-H. Chung, *Nanoscale* 4 (2012) 568–575.
- [19] S. Cherevko, C.-H. Chung, *Electrochim. Commun.* 13 (2011) 16–19.
- [20] S. Cherevko, N. Kulyk, C.-H. Chung, *Langmuir* 28 (2012) 3306–3315.
- [21] H. Mukaibo, T. Momma, T. Osak, *J. Power Sourc.* 146 (2005) 457–463.
- [22] J.G. Kim, S.H. Lee, S.H. Nam, S.M. Choi, W.B. Kim, *RSC Adv.* 2 (2012) 7829–7836.